JOURNAL OF SOLID STATE CHEMISTRY 6, 195–202 (1973)

Direct Observation of the Formation of Double-Shear Structures from Nb_3O_7F

L. A. BURSILL

School of Chemistry, University of Western Australia, Nedlands, 6009, Australia

Received May 10, 1972

It is shown that slight decomposition of Nb_3O_7F occurs readily in the beam of an electron microscope. Planar faults are produced on at least five different (*hkl*) planes. These grow into the crystal from the surface by expansion of partial dislocations. Further decomposition requires much higher beam heating and results in complete recrystallization and void formation giving a poorly ordered double-shear structure based on Nb_3O_7F. It is suggested that the first stage involves some reduction of Nb^{5+} with release of oxygen and/or fluorine whereas the different mechanism of the second stage follows from the evolution of $NbOF_3$, a reaction which does not occur by a simple solid state mechanism.

Introduction

The niobium oxyfluoride NbO_2F decomposes, in a stream of argon or in vacuum, by two stages (*1*),

$$4NbO_2F \xrightarrow{600-750^\circ C} Nb_3O_7F + NbOF_3(g) \quad (1)$$

$$3Nb_3O_7F \xrightarrow{800-1300^\circ C} 4Nb_2O_5 + NbOF_3(g). \quad (2)$$

Nb_3O_7F is a crystallographic shear (*CS*) structure M_nO_{3n-1}($n = 3$) derived from NbO_2F (ReO_3-type) by the *CS* operation $(100)_R\frac{1}{2}[1\bar{1}0]_R$ (*2*). Nb_2O_5 has many polymorphs but the final product, above 1300°C, is H–Nb_2O_5 which may be derived from Nb_3O_7F by the introduction of a second set of *CS* planes intersecting the first (*3*). Four oxyfluorides, $Nb_{31}O_{77}F$ and $Nb_{17}O_{42}F$ (*4*) and $Nb_{59}O_{147}F$ and $Nb_{65}O_{161}F$ (*5*), have been prepared by heating mixtures of Nb_3O_7F and Nb_2O_5 in sealed platinum capsules. These are also double-shear structures based on Nb_3O_7F (*6*). A further phase $Nb_5O_{12}F$, of unknown structure, was also reported (*7*).

A simple solid state diffusion mechanism was proposed for the first reaction (*8*) but direct observation by beam heating in the electron microscope (*9*) showed that the real situation is more complex. Reduction to $NbX_{2.999}$ occurs readily at low beam heating by the expansion of partial dislocation loops, apparently confirming the suggestion (*10*) that a dislocation mechanism would operate in such cases. Further decomposition required much higher beam heating, when grainy crystallites of disordered Nb_3O_7F were obtained. Voids and considerable recrystallization occurred and there was not, in general, a simple habit relationship with the original single crystal flake [see Fig. 4 in (*9*)]. No intermediate compounds M_nX_{3n-1} ($4 \leqslant n \leqslant \infty$) could be found. Once initiated this stage of the decomposition was extremely rapid.

The diffusion and dislocation mechanisms may both be extended to provide models for reaction (2) [see for example in (*11*)]. But, as in the case of Eq. (1), neither model takes into account the necessary change in oxygen/fluorine ratio in the solid due to the release of $NbOF_3$. It was admitted (*11*) that some elaboration is required and suggested that cracks may occur so that $NbOF_3$ molecules could diffuse to the surface.

Further electron microscope results are now reported in an attempt to observe the mechanism of formation of double-shear structures from Nb_3O_7F. These also help to clarify the role of $NbOF_3$.

Experimental Methods

Colorless crystals of Nb_3O_7F up to 1 mm long were grown by mixing equimolar amounts of NbO_2F and $H\text{–}Nb_2O_5$, sealing in platinum capsules and heating at 800°C for 2 days. Both the starting and product crystals were identified using Guinier powder photographs. Fragments of crystal were fractured between glass slides,

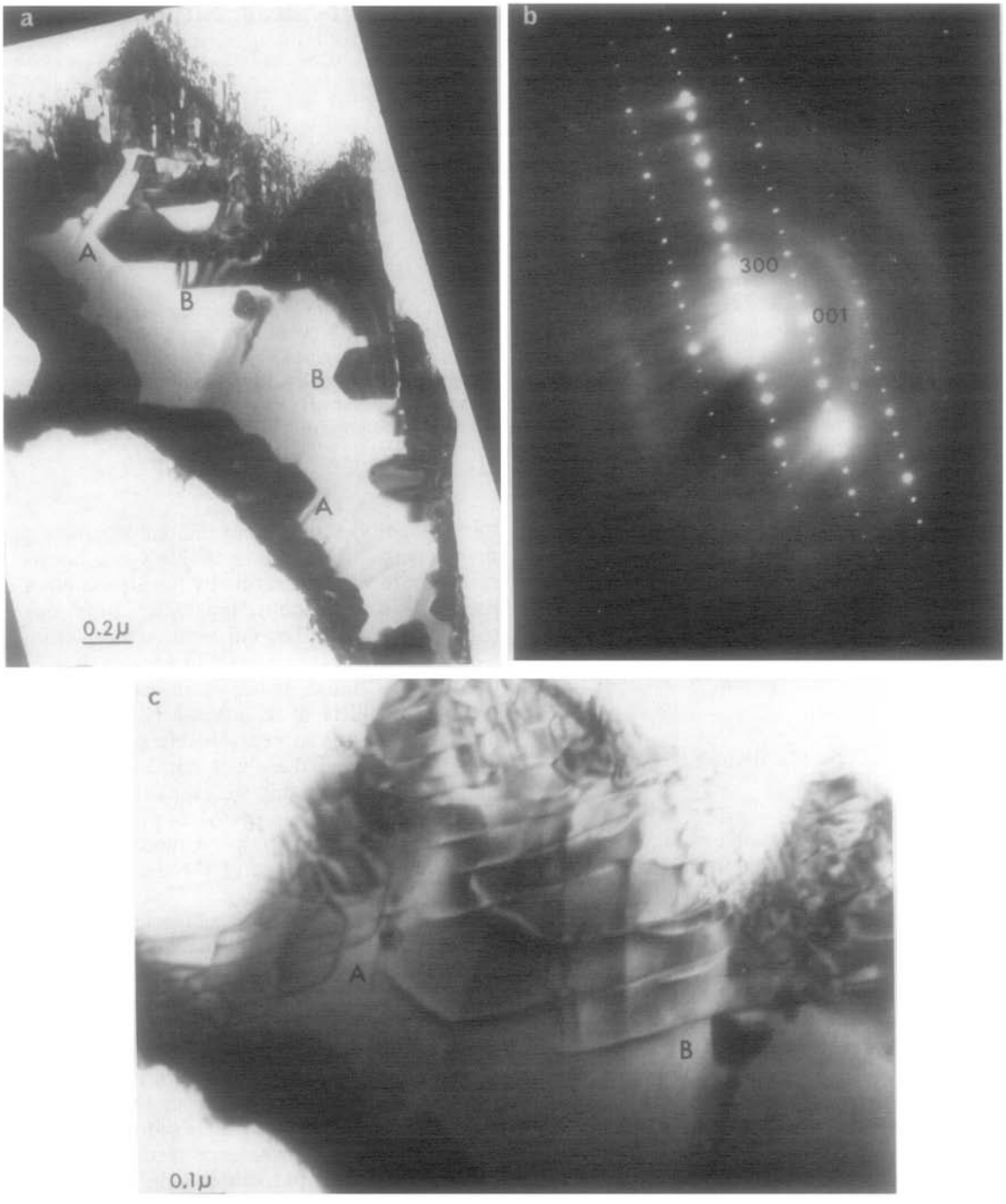

FIG. 1a. Nb_3O_7F flake after pulse heating in the electron beam. Note the dark crystal-shaped areas at (A) and (B). (b) Diffraction pattern of (a) showing [010] zone. (c) Enlargement of top of (a) after tilting so that the one strong reflection was 11,2,2.

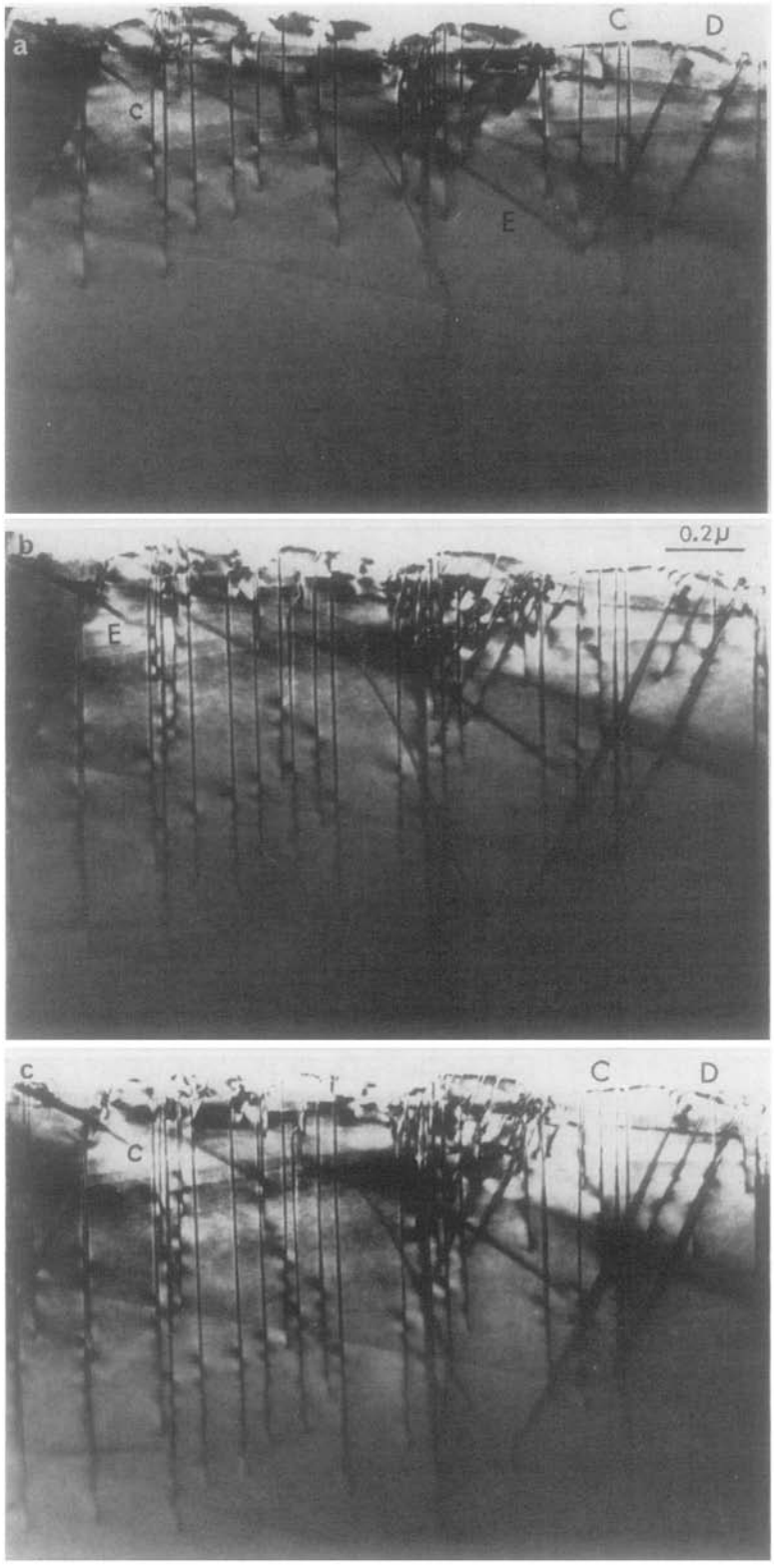

FIG. 2a, b, c. Time-lapse sequence of Nb_3O_7F crystal after three successive pulse heatings. Note oscillatory contrast at the end of each dark line. (C and D) parallel to (010) and (310), (E) is the edge of the carbon film.

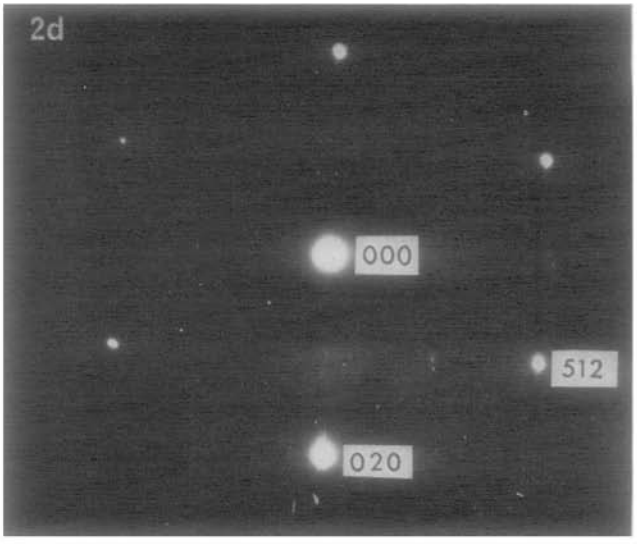
2d
000
512
020

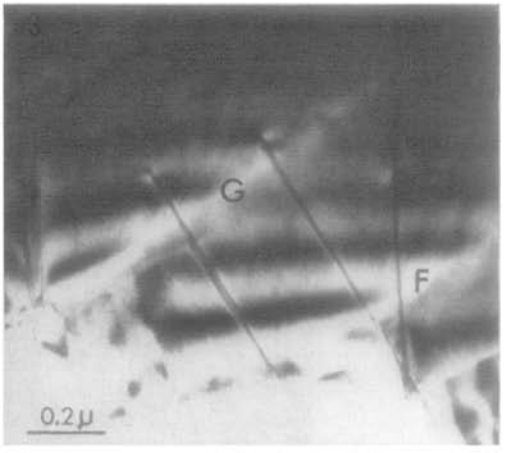
G
F
0.2μ

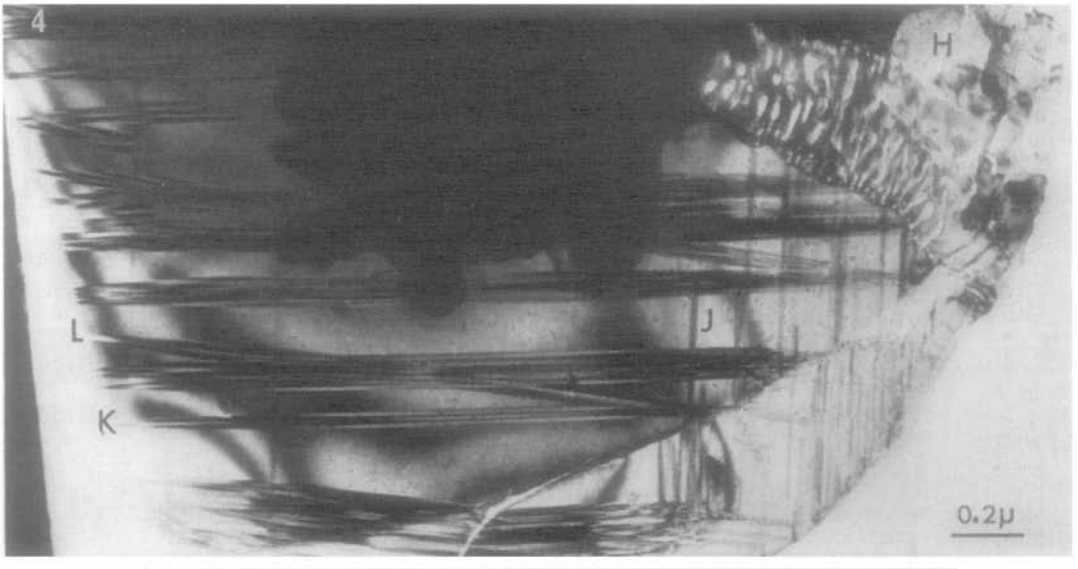
4
H
L
J
K
0.2μ

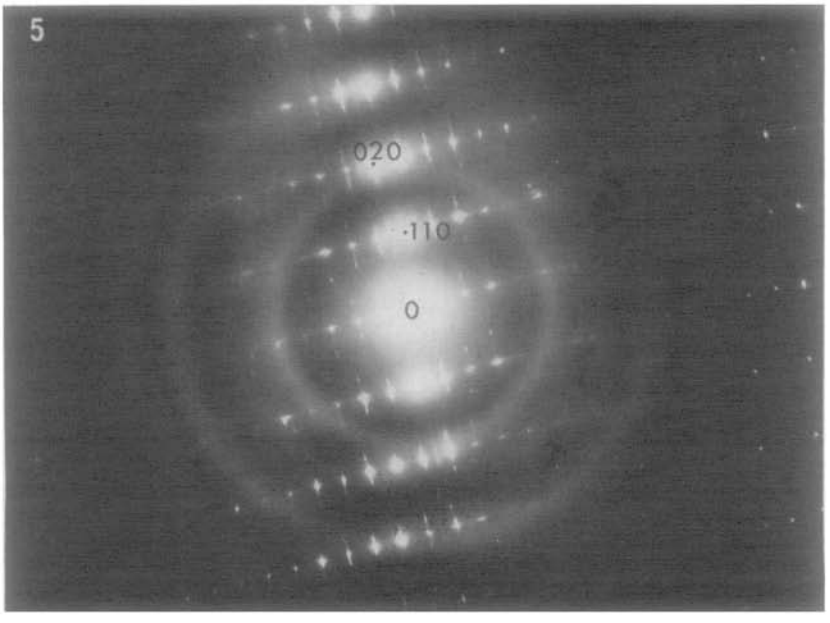
5
020
·110
0

mounted on carbon support films and examined in a JEM-6A electron microscope using a goniometer stage. Direct observation of the decomposition was made by removing the condenser aperture and switching off the first condenser lens, giving a very high beam intensity if desired. With care, some measure of control over the reaction rate could be achieved. Preliminary experiments confirmed that Nb_3O_7F did not suffer radiation damage at normal beam intensities.

Observations

Figure 1a shows a flake of Nb_3O_7F after pulse heating in the electron beam. Black crystal-shaped areas are shown (A, B); these grew into the initially featureless crystal, starting at the edges. The corresponding diffraction pattern (Fig. 1b) shows the [010] zone axis so that (010) planes lie in the plane of Fig. 1a (Nb_3O_7F is orthorhombic with $a = 20.67$ Å, $b = 3.833$ Å and $c = 3.927$ Å). Figure 1c shows this same area after tilting so that 11,2,2 was the only strong operating reflection. Asymmetrical line contrast now outlines the areas (A, B) which were dark in Fig. 1a.

Figure 2a, b, c show a time-lapse sequence of a Nb_3O_7F crystal after three successive pulse heatings. Line contrast is seen extending into the crystal from the surface. These increase in length approximately uniformly after each pulse. Note the oscillatory contrast at the end of each line. The diffraction conditions are given in Fig. 2d where the strong reflections are 020, 512 and $5\bar{1}2$. Lines (C) (Fig. 2a) have trace parallel to (010) while the fringes (D) make apparent angle 28° to (010). The lines are not all perfectly straight or perfectly parallel. Lines (E) are artifacts due to the edge of the carbon support film.

Two sets of line features were produced in a third crystal (Fig. 3). In this case the plane of the specimen was (001) and one set (F) is parallel to (010) while the second (G) is at 30° to this, i.e., parallel to (310).

Attempts to produce a higher density of defects always resulted in a vigorous recrystallization of the specimen. For instance Fig. 4 shows a recrystallized area (H), containing voids, advancing on an area containing a low density of fringes at (J, K, and L). Diffraction patterns from recrystallized areas showed intense streaking normal to (010) and also at a slight angle to this (Fig. 5).

Interpretation

The above observations clearly establish that planar faults are produced in Nb_3O_7F after it is heated in the electron beam. The fault planes are predominantly (010) but others occurred. Thus the uniform areas (A) in Fig. 1a are (010) faults lying in the plane of the photograph while the black lines in Fig. 2 represent (010) faults seen edge-on at (C). The fringes (D) in Fig. 2 are due to faults inclined to the electron beam. Trace analysis shows they are on (310) planes, which in Fig. 2 are inclined at 25° to the beam and make apparent angle 28° to the trace of (010). The two sets of faults seen edge-on in Fig. 3 are parallel to (010) (F) and (310) (G). Three sets of faults (J, K, L) in Fig. 4 index as (100), (110) and $(1\bar{1}0)$, respectively. Faults at (B) in Fig. 1a show wide fringe contrast and therefore dip at a shallow angle to the plane of the photograph, presumably because they line on (110) or $(1\bar{1}0)$ planes. The diffraction pattern (Fig. 5) shows that a high density of disordered (010) faults occurred in the recrystallized areas. Altogether five different fault planes were observed, i.e., (010), (110), $(1\bar{1}0)$, (310) and (100).

Attempts to determine the fault vectors R_i by diffraction contrast analysis were not successful due to the large number of different fault planes, the sensitivity of the specimens to the beam and the difficulty, for crystals with a long axis, to obtain two-beam conditions. A large number of these would be required as we expect the fault vectors to be nonideal (*12*).

Whenever fault growth was directly observed it occurred by the expansion of a partial dislocation into the crystal from the surface (Figs. 1, 2). The dislocation is revealed as asymmetrical line contrast if it lies in the plane of the figure (Fig. 1c) or by oscillatory contrast if inclined to the electron beam (Fig. 2) (*13*). The faults are out of

FIG. 2d. Diffraction conditions for Fig. 2a, b, c, zone axis [20$\bar{5}$].

FIG. 3. Nb_3O_7F flake containing (010) (F) and (310) (G) faults edge-on.

Fig. 4. A recrystallized area (H) advancing on area containing a low density of (100) (J), (110) (K), and $(1\bar{1}0)$ (L) faults.

FIG. 5. Diffraction pattern from a recrystallized area showing streaking approximately normal to (010).

contrast in Fig. 1c whereas the dislocations are not. Fault contrast is extinguished for $g \cdot R = N$, where g is the reciprocal lattice vector of the operating reflection (two-beam case) and N is *any* integer, including zero. On the other hand dislocation contrast may occur for $g \cdot R$ equal to an integer other than zero (*13*), which is therefore the case in Fig. 1c.

Discussion

The oxyfluorides $Nb_{31}O_{77}F$, $Nb_{17}O_{42}F$, $Nb_{59}O_{147}F$ and $Nb_{65}O_{161}F$ all have *CS* planes with indices (101) when referred to Nb_3O_7F [see Ref. (*6*) Fig. 3]. This is not one of the faults observed above, possibly because these phases formed only in sealed tubes at higher temperatures than required to decompose Nb_3O_7F.

Andersson proposed (*11*) that N-Nb_2O_5 was an intermediate product in the decomposition and suggested a solid state diffusion mechanism, involving the sideways movement of *CS* planes into Nb_3O_7F. However N-Nb_2O_5 is a 4×4 ReO_3-type block structure and does not appeal as a natural intermediate between Nb_3O_7F and H-Nb_2O_5 which have $3 \times \infty$ and (3×4, 3×5) ReO_3-type blocks respectively. Referred to Nb_3O_7F indices N-Nb_2O_5 has orthogonal *CS* planes (100) and (001). The first is present in Nb_3O_7F but the second was not observed above. Note however that the predominant fault (010) is also orthogonal to (100).

Andersson (*14*) has systematized many other possible ways to shear Nb_3O_7F and his group $B_1C_{m,n}$ does encompass a set of *CS* planes whose indices correspond with the faults observed above. The [001] projection of Nb_3O_7F and the four *CS* planes (010), (110), (210) and (310) are drawn in Fig. 6. In each case the shear vector is $\frac{1}{2}[011]$ and the *CS* plane may be formally imagined to be produced by removing a set of anions and shearing by an octahedral edge.

Two possibilities arise for the (100) faults. If we insert an additional $(100)[\frac{1}{10}\ \frac{1}{2}\ 0]$ *CS* plane into Nb_3O_7F (Fig. 7a) and one adjacent *CS* plane moves sideways (Fig. 7b) we obtain a lamellar of R-Nb_2O_5 (*15*). If instead we carry out a similar operation with vector $[\frac{1}{10}\ 0\ \frac{1}{2}]$ we obtain a lamellar of P-Nb_2O_5 (*16*), in which $(100)[\frac{1}{10}\ \frac{1}{2}0]$ and $(100)[\frac{1}{10}\ 0\ \frac{1}{2}]$ alternate (Fig. 7c). Note that $(100)\ [\frac{1}{10}\ \frac{1}{2}\ 0]$ may be converted to $(100)[\frac{1}{10}\ 0\ \frac{1}{2}]$ by the passage across it of a partial dislocation having Burgers vector $\frac{1}{2}[01\bar{1}]$. This anti-phase boundary operation thus provides a possible mechanism relating R-Nb_2O_5 and P-Nb_2O_5.

It is also interesting to note that (*hk*0) *CS* planes (Fig. 6) may be resolved as

$$(hk0) = p \cdot (010) + q \cdot (100),$$

where p and q are integers. Thus any high index *CS* plane (*kh*0) may be obtained by varying the ratio p/q. That some (010) faults in Fig. 2 are not perfectly straight or parallel is then explained by assuming a small admixture of (100) [see also the streaking in Fig. 5 which is not always exactly normal to (010)]. (210) *CS* planes are more complex in the sense that they involve ordered intergrowth of (110) and (310) (Fig. 6d) and Figs. 2 and 3 suggest that these are not stable.

Of course the structures drawn in Figs. 6 and 7 must be regarded as speculative as the shear vectors could not be determined experimentally. Extinction of the faults but not the dislocations in Fig. 1c is consistent with vector $\frac{1}{2}[011]$ because for $g(11,2,2)$ $g \cdot R = 2.0$.

Regardless of the precise structure of the faults it is clear that a simple diffusion mechanism (*8*, *11*) does not operate. In fact a low density of faults, on five different planes, is readily produced by expansion of partial dislocations into the crystal from the surface. The density of faults, assuming they are *CS* planes, corresponds to reduction of the anion/metal ratio by less than 0.001, i.e., very much less than the 0.167 required to produce Nb_2O_5. Further decomposition required much higher beam intensities and involved drastic recrystallization (Fig. 4). It occurred extremely rapidly, on pulse heating for about 1 sec, and in effect must be equivalent to a vapor phase transport reaction where the product is deposited in the proximity of the original crystal. Thus there is not necessarily a simple habit relation between reactant and product [see Fig. 4 and also Fig. 4 in (*9*)]. As crystal growth occurred extremely rapidly we might expect that the products will not be well ordered, either in spacing or orientation of the *CS* planes.

In principle any of the observed fault planes could give rise to a homologous series of structures between Nb_3O_7F and Nb_2O_5. The diffraction patterns (Fig. 5) showed that the recrystallized product contained a high density of disordered (010) faults. The stoichiometry could not be estimated. This double-shear structure does contain ReO_3-type blocks three octahedra wide and is a reasonable intermediate stage to the production of H-Nb_2O_5 at higher temperatures.

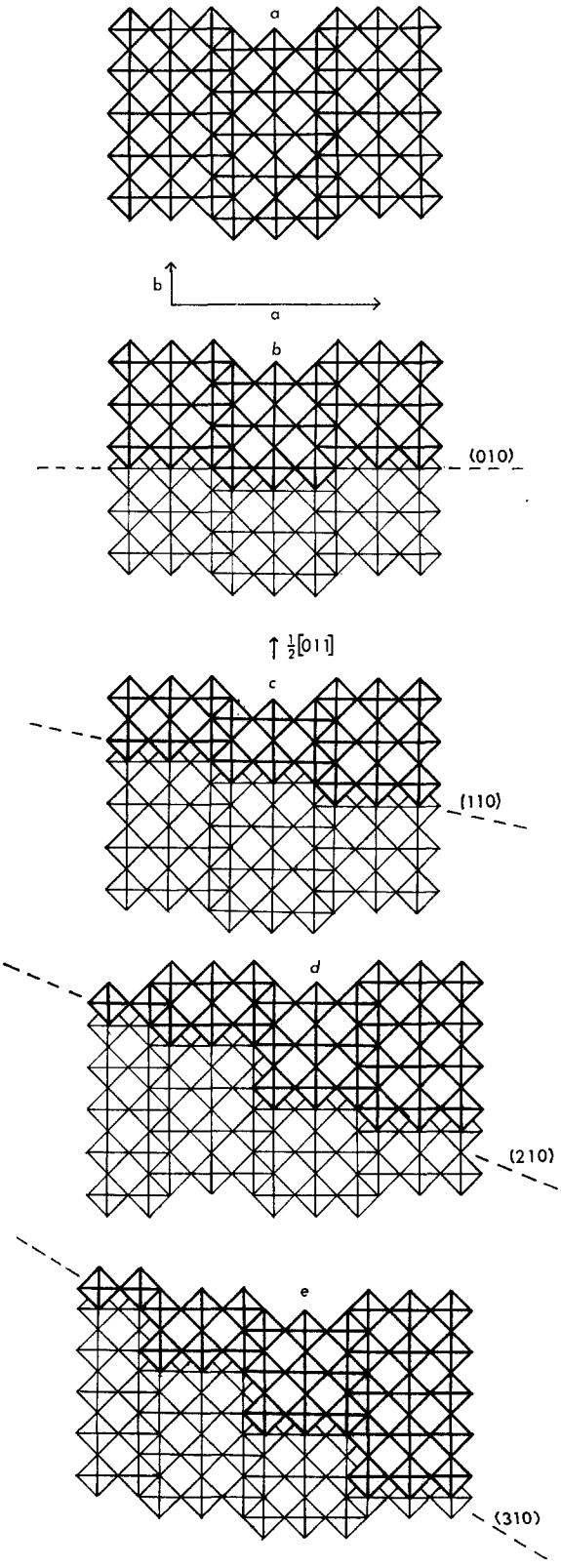

In many respects the decomposition of Nb_3O_7F closely parallels the observations for NbO_2F (*9*). Both appear to have two distinct stages.

1. The production of a very low density of *CS* planes on a number of different (*hkl*) planes. This occurs at low beam heating by a solid state mechanism involving the extension of partial dislocations.

2. The production, at higher beam heating, of a grainy recrystallized material containing voids, which in general does not have a simple habit relation to the reactant. The product was poorly ordered, being Nb_3O_7F for reaction (1) or a double-shear structure derived from Nb_3O_7F for Eq. (2).

Reactions (1) and (2) are quite unlike those of some oxide systems where a very large number of ordered intermediate structures occur, see for instance Ti_nO_{2n-p} (*17*). Here there are two very big jumps in anion/metal ratio, from 3.000 to 2.66$\dot{6}$ and from 2.66$\dot{6}$ to 2.500. Reduction of TiO_x may occur continuously by the loss of oxygen from the surface and the diffusion of Ti^{3+} into the crystal, either along the dislocation bounding new *CS* planes for $2.00 \geqslant x \geqslant 1.93$ and $1.89 \geqslant x \geqslant 1.75$, or along the existing *CS* planes causing them to rotate from (132) to (121) for $1.93 \geqslant x \geqslant 1.89$ (*17*). On the other hand in the oxyfluorides $NbOF_3$ is lost from the solid and this demands overall adjustment of the oxygen/fluorine ratio throughout the crystal. While it is possible that this could be achieved by a complex highly regimented solid state diffusion mechanism the observations show that this does not occur in the electron microscope. Instead we see a vigorous reconstruction of the crystal best described as a vapor phase reaction. Under these circumstances there is no coherence between reactant and product and it is not possible to stop the reaction at any stage. In addition to this kinetic factor there must also be thermodynamic reasons favoring Nb_3O_7F and Nb_2O_5 as products rather than the many other geometrically possible intermediate structures.

The very slight degree of reduction in anion/metal ratio which occurs in both Nb_3O_7F and NbO_2F at relatively low beam intensities does proceed continuously and involves the same type of dislocation mechanism as occurred in other

Fig. 6a. Idealized [001] projection of Nb_3O_7F. (b) (010)½[011] *CS* plane in Nb_3O_7F; (c) (110)½[011] *CS* plane in Nb_3O_7F; (d) (210)½[011] *CS* plane in Nb_3O_7F; (e) (310)½[011] *CS* plane in Nb_3O_7F.

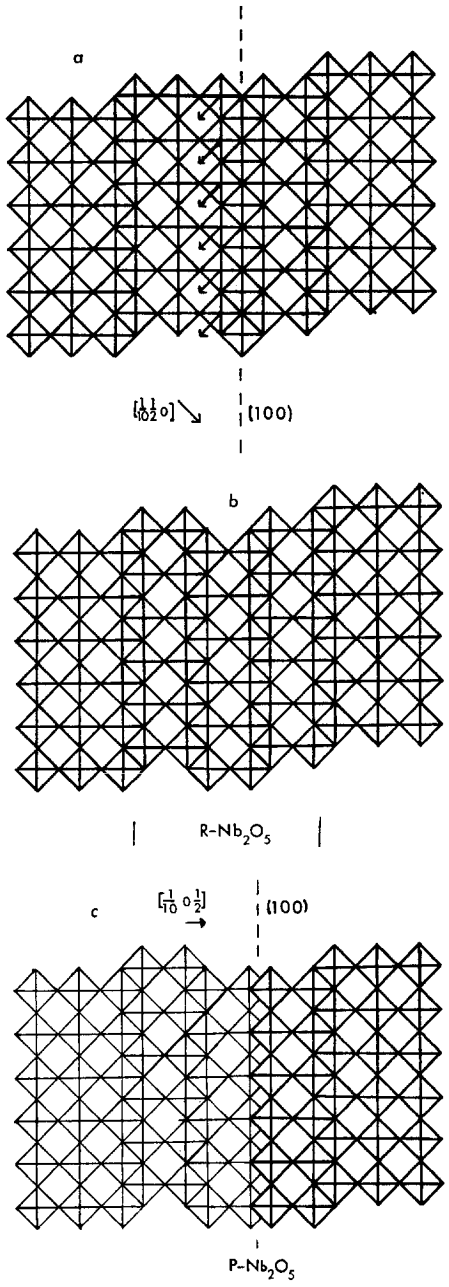

FIG. 7a. (100) $[\frac{1}{10}\ \frac{1}{2}\ 0]$ *CS* plane in Nb_3O_7F. Arrows indicate movement of [MO] strings required to shift an existing *CS* plane sideways. (b) Lamellar of R-Nb_2O_5 resulting from atom jumps shown in Fig. 7a. (c) Result of inserting a (100) $[\frac{1}{10}\ 0\ \frac{1}{2}]$ *CS* plane Nb_3O_7F. Note the lamellar of P-Nb_2O_5.

oxide systems (*17–19*). It is therefore suggested that there is slight reduction of Nb^{5+} to Nb^{4+} with consequent loss of oxygen and/or fluorine from both NbO_2F and Nb_3O_7F under these conditions. Evolution of $NbOF_3$, which does not involve the reduction of Nb^{5+}, occurs only at higher temperatures. Preparation of Nb_3O_7Cl in the absence of any oxidizing agents (*20*) results in blue rather than colorless crystals. Blue crystals of Nb_3O_7F were also obtained in some preparations in our laboratory (*21*).

The observation of several unsuspected (*hkl*) *CS* planes in Nb_3O_7F adds to mounting electron microscope evidence (*17*, *18*, *19*) that the *CS* planes in slightly reduced crystals may be quite different to those found by X-ray diffraction in ordered structures at very much greater degrees of reduction.

Acknowledgments

Financial support for this work was given by the Australian Research Grants Committee, the University of Western Australia and AFOSR Grant No. AF-AFOSR-835-67, United States Air Force.

References

1. S. ANDERSSON AND A. ÅSTRÖM, *Acta Chem. Scand.* **19**, 2136 (1965).
2. S. ANDERSSON, *Acta Chem. Scand.* **18**, 2339 (1964).
3. B. GATEHOUSE AND A. D. WADSLEY, *Acta Crystallogr.* **17**, 1545 (1964).
4. S. ANDERSSON, *Acta Chem. Scand.* **19**, 1401 (1965).
5. R. GRUEHN, *Naturwissenschaften* **54**, 645 (1967).
6. A. ÅSTRÖM, *Acta Chem. Scand.* **20**, 969 (1966).
7. S. ANDERSSON AND A. ÅSTRÖM, *Acta Chem. Scand.* **18**, 2233 (1964).
8. S. ANDERSSON AND A. D. WADSLEY, *Nature (London)* **211**, 581 (1966).
9. L. A. BURSILL AND B. G. HYDE, *Phil. Mag.* **20**, 657 (1969).
10. J. S. ANDERSSON AND B. G. HYDE, *J. Phys. Chem. Solids* **28**, 1393 (1967).
11. S. ANDERSSON, *Ark. Kemi* **26**, 521 (1967).
12. L. A. BURSILL AND B. G. HYDE, *Proc. Roy. Soc., Ser. A* **320**, 147 (1970).
13. P. B. HIRSCH, A. HOWIE, R. B. NICHOLSON, D. W. PASHLEY, AND M. J. WHELAN, "*Electron Microscopy of Thin Crystals*," Butterworths, London (1965).
14. S. ANDERSSON, *Bull. Soc. Chim. Fr.*, p. 1088 (1965).
15. R. GRUEHN, *J. Less-Common Metals* **11**, 119 (1966).
16. W. PETTER AND F. LAVES, *Naturwissenschaften* **52**, 617 (1965).
17. L. A. BURSILL AND B. G. HYDE, *Progr. Solid State Chem.* 7, 177 (1972).
18. L. A. BURSILL, *Proc. Roy. Soc. Ser. A* **311**, 267 (1969).
19. J. G. ALLPRESS, R. J. D. TILLEY, AND M. J. SIENKO, *J. Solid State Chem.* **3**, 440 (1971).
20. H. SHÄEFER, E. SIBBING, AND R. GERKEN, *Z. Anorg. Allg. Chem.* **307**, 163 (1961).
21. S. CORONEOS, thesis, University of Western Australia, 1970.